JOURNAL OF THERMOPHYSICS AND HEAT TRANSFER
Vol. 20, No. 4, October–December 2006

# Numerical Modeling of Near-Continuum Flow over a Wedge with Real Gas Effects

Yevgeniy A. Bondar*
*Institute of Theoretical and Applied Mechanics, 630090, Novosibirsk, Russia*
Gennady N. Markelov†
*Advanced Operations and Engineering Services, 2332 KG Leiden, The Netherlands*
Sergey F. Gimelshein‡
*University of Southern California, Los Angeles, California 90089*
and
Mikhail S. Ivanov§
*Institute of Theoretical and Applied Mechanics, 630090, Novosibirsk, Russia*

DOI: 10.2514/1.18758

**Effects of vibrational relaxation and dissociation on the standoff distance of the bow shock wave on a wedge are numerically examined with the use of the kinetic (DSMC method) and continuum (Navier–Stokes equations) approaches. A hypersonic flow around the wedge is computed for Knudsen numbers about $5 \times 10^{-4}$ in a wide range of wedge angles both for a monatomic gas (argon) and a diatomic reacting and nonreacting gas (nitrogen). DSMC computations are based on three different real gas effect models. The kinetic and continuum results for the standoff distance are in good agreement for argon and nonreacting nitrogen. The influence of vibration-dissociation coupling on the results of numerical simulations is analyzed. Sensitivity of simulation results to chemical reaction rate constants is also estimated. Numerical simulations show that dissociation is responsible for the nonlinear form of the dependence of the standoff distance on the wedge angle, which qualitatively agrees with available experimental data.**

## Nomenclature

| | | |
|---|---|---|
| $E_d$ | = | dissociation energy of molecule, J |
| $e$ | = | internal energy, J/kg |
| $h$ | = | enthalpy, J/kg |
| $Kn$ | = | Knudsen number based on the wedge length, $w$ |
| $L$ | = | wedge spanwise dimension, m |
| $M$ | = | Mach number |
| $p$ | = | pressure, Pa |
| $Re$ | = | Reynolds number based on the wedge length, $w$ |
| $T$ | = | temperature, K |
| $T_r$ | = | rotational temperature, K |
| $T_t$ | = | translational temperature, K |
| $T_v$ | = | vibrational temperature, K |
| $T_x$ | = | parallel temperature, K |
| $T_y$ | = | perpendicular temperature, K |
| $V$ | = | velocity, m/s |
| $w$ | = | length of a wedge, m |
| $\gamma$ | = | specific heat ratio |
| $\delta_w$ | = | wedge half-angle, deg |
| $\lambda$ | = | gas mean free path, m |
| $\xi$ | = | average number of effective degrees of freedom |
| $\rho$ | = | density, kg/m$^3$ |
| $\phi$ | = | parameter of vibration-dissociation coupling |

*Subscript*

| | | |
|---|---|---|
| $\infty$ | = | freestream value |

## Introduction

THE direct simulation Monte Carlo (DSMC) method is traditionally used to study rarefied hypersonic flows with a significant degree of thermal and chemical nonequilibrium. The method has been successfully applied to study various problems of high-altitude aerothermodynamics. Presently, one of the most challenging problems in terms of the method development and improvement is related to the need to effectively and reliably simulate processes of energy transfer between internal and translational modes and chemical reactions. The real gas effects such as the excitation of internal degrees of freedom and chemical reactions in the gas phase considerably change flow properties and surface parameters, which stimulates the development of physically realistic DSMC models of real gas effects.

Many models of the internal energy transfer and chemical reactions were suggested in the literature (see, for example, [1–5] and references therein). The models differ in the area of applicability, derivation, and accuracy. A detailed review may be found in [6,7]. Let us mention here only the most important issue related to all DSMC models for the internal energy transfer and chemical reactions. Whereas the energy dependent cross sections of these processes may not be known from experiment or theoretical analysis, the corresponding temperature-dependent rates are often known with an acceptable accuracy. It is therefore critical for the DSMC models to reproduce the known temperature dependence. For the internal energy transfer, it is usually sufficient to match the rotational and vibrational relaxation governed by the Jeans and Landau–Teller equations with temperature-dependent rotational and vibrational relaxation numbers $Z_r$ and $Z_v$, respectively. For chemical reactions, it is necessary to match the Arrhenius reaction rates at equilibrium.

Currently, there is a lack of models that are general enough to treat various molecular interactions and processes, sufficiently accurate to capture complex flow physics and preserve proper thermal relaxation

Presented as Paper 1183 at the 42nd AIAA Aerospace Sciences Meeting and Exhibit, Reno, NV, 5–8 January 2004; received 25 July 2005; revision received 27 October 2005; accepted for publication 27 October 2005. 

*Associate Research Scientist, Institutskaya 4/1. Member AIAA.
†Senior Aerospace Engineer, Haagse Schouwweg 6G. Member AIAA.
‡Research Assistant Professor, 201 Rapp Research Building. Member AIAA.
§Professor, Head of CFD Lab, Institutskaya 4/1. Associate Fellow AIAA.

and chemical rates, easy to implement, and computationally efficient to be applied to simulate near-continuum flows. The Larsen–Borgnakke (LB) model [8] is the most common in the DSMC method for the translational-internal energy exchange. The key advantage of this model is that it is relatively simple and can be applied to polyatomic molecules. Both continuous and discrete representations of rotational and vibrational energy of molecules in the LB model are currently used in the DSMC method. As was shown in [9], the use of discrete models in the DSMC method is preferable. The use of a particle selection methodology and DSMC corrections for the rotational [10] and vibrational [11] relaxation numbers enables one to maintain Jeans and Landau–Teller relaxation rates.

The chemical reactions are usually taken into account in the DSMC method using the total collision energy (TCE) model derived for continuous internal energies [12]. The combination of the LB model for continuous internal energies with the TCE model will be further called in this paper the "continuous model of real gas effects." The TCE model of chemical reactions was modified in [9] to accommodate discrete internal energies; the new model allows one to match experimental reaction rates at equilibrium. The model is used in this work with the discrete Larsen–Borgnakke model for the energy transfer between translational and internal modes. Both rotational and vibrational modes were discrete in this case, and the use of a selection methodology prohibiting double relaxation allowed us to maintain correct energy transfer and chemical rates. This model is denoted as "discrete model of real gas effects" hereafter. Recently the modification procedure of [9] was applied to the model which takes into account the effect of vibration-dissociation coupling (VDC) [1]. This model also employs the discrete description of internal energy of molecules, also is used with the discrete Larsen–Borgnakke model and will be further called "VDC model of real gas effects." An important step for the application of the new models is their verification and validation.

The verification of the models is relatively straightforward and has already been performed for the homogeneous heat bath conditions [13]. Their validation, however, is much more difficult due to the lack of experimental data on rarefied hypersonic reacting flows. The lack of data is principally related to the complexity of experimental studies of high-enthalpy rarefied flows in ground-based facilities. As a result, most of currently available experimental conditions pertain to high-density, continuum flows, with the Knudsen number ranging typically from $10^{-5}$ to $10^{-6}$.

An example of the scarce data suitable for validation of real gas effect models for the DSMC method is the experimental results presented in [14]. Principal attention was paid to the effects of thermal relaxation and dissociation on the shock wave standoff distance for a flow about a wedge placed symmetrically in a uniform hypersonic flow. Near-continuum flows of argon, dissociating nitrogen, and dissociating carbon dioxide over a wedge with $Kn \sim 5 \times 10^{-4}$ were examined there, providing therefore good grounds for the DSMC model validation.

The principal goal of this work is the validation of the DSMC models of real gas effects by an example of a hypersonic flow over a wedge in the near-continuum flow regime. For this purpose, DSMC computations of an argon flow and also nonreacting and reacting nitrogen flows were performed with three different models of real gas effects, and the results on the shock wave standoff distance were compared with the experimental data [14]. In addition, Navier–Stokes (NS) computations were performed for these flows, and the results were compared with the DSMC predictions.

## Flow Conditions

A wedge of a length $w = 0.051$ m was used in the experiments of [14]. Because the wedge spanwise dimension was $L = 0.152$ m, the flow in the symmetry plane may be considered as two-dimensional. A 2-D statement was used, therefore, in the present study.

The freestream conditions are listed in Table 1. The values of the main parameters (velocity, temperature, density, and flow composition) were taken from [14]. Based on these four parameters, all the remaining parameters listed in Table 1 were calculated.

**Table 1 Freestream conditions**

| | Argon | Nitrogen |
|---|---|---|
| $V_\infty$, m/s | 2,200 | 5,500 |
| $T_\infty$, K | 57 | 1,100 |
| $p_\infty$, Pa | 26.11 | 940.3 |
| $\rho_\infty$, kg/m$^3$ | 0.022 | 0.026 |
| $M_\infty$ | 15.64 | 7.7 |
| $Kn_\infty$ | $4.7 \times 10^{-4}$ | $6.52 \times 10^{-4}$ |
| $Re_\infty$ | 41,500 | 14,485 |
| Composition, mol/kg | Ar 25 | $N_2$ 31.9<br>N 7.7 |

The following dissociation reactions were taken into account in studying the chemically reacting nitrogen flow both in DSMC and NS computations:

1)

$$N_2 + N_2 \rightarrow N + N + N_2$$

$$(E_d = 1.561 \times 10^{-18}\ \text{J}, A = 4.797 \times 10^{17}\ \text{cm}^3 \cdot \text{mol}^{-1} \cdot \text{s}^{-1}, B = -0.5)$$

2)

$$N_2 + N \rightarrow N + N + N$$

$$(E_d = 1.561 \times 10^{-18}\ \text{J}, A = 4.154 \times 10^{22}\ \text{cm}^3 \cdot \text{mol}^{-1} \cdot \text{s}^{-1}, B = -1.5)$$

Here, $A$ and $B$ are constants in the Arrhenius equation (the values are taken from [15])

$$k_d = AT^B \exp\left(-\frac{E_d}{kT}\right) \tag{1}$$

To assess the sensitivity of the computational results to the choice of chemical reaction rates, an alternative set of reaction rates [16] was used in additional DSMC computations: $A = 2.3 \times 10^{29}$ cm$^3 \cdot$ mol$^{-1} \cdot$ s$^{-1}$, $B = -3.5$ for the first reaction and $A = 8.491 \times 10^{25}$ cm$^3 \cdot$ mol$^{-1} \cdot$ s$^{-1}$, $B = -2.5$ for the second reaction.

The recombination reactions were not modeled in the present study. Under given conditions, recombination occurs in the boundary layer only, which will be demonstrated next.

## Computational Methods

### DSMC Method

The DSMC computations were performed using the SMILE software system [17] developed at the Institute of Theoretical and Applied Mechanics (ITAM, Novosibirsk) and based on the majorant frequency scheme. SMILE employs two independent grids adapted in the course of computation: the first one to organize particle collisions, and the second one for sampling of macroparameters. Both grids are based on uniform rectangular background cells, which are split into smaller cells, if necessary.

The following models were employed in the computations:

1) Variable soft sphere (VSS) molecular collision model [2] with VSS parameters from [12].

2) Diffuse reflection model with complete accommodation of translational and internal energies at the wedge surface.

3) Three models of real gas effects, namely, a) continuous model (LB model for the translational-internal energy transfer and conventional TCE model for chemical reactions), b) discrete model (LB model for the translational-internal energy transfer and modified TCE model [9] for chemical reactions), and c) VDC model (LB model for the translational-internal energy transfer and modified VDC model [13] for chemical reactions).

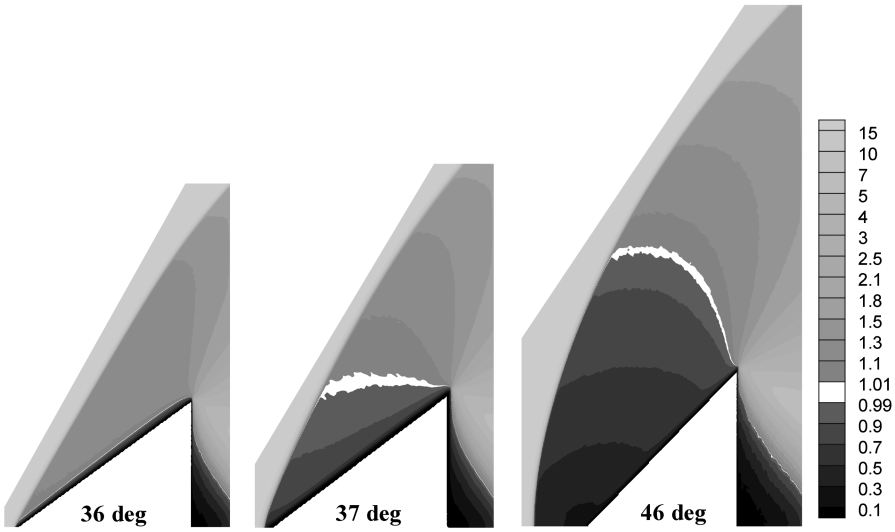


**Fig. 1 Mach number flowfields for different wedge angles (argon flow).**

4) Temperature-dependent rotational and vibrational collision numbers in all models of real gas effects for modeling translational-rotational and translational-vibrational energy transfer.

Note that discrete and VDC models differ only in the form of chemical reaction probability function and in case of nonreacting flow both models are identical. Hence only continuous and discrete models are considered for nonreacting nitrogen flow.

#### Solution of NS Equations

NS computations are performed with a commercial software, CFD-FASTRAN, which is a compressible finite-volume flow solver [18]. The software provides advanced features including 6-DOF modeling for simulating the unsteady, dynamic motion of multibody configurations and thermochemistry for reacting flows.

The following features of CFD-FASTRAN are used in the present paper: 1) structured grid solver; 2) Roe's approximate Riemann solver as a flux difference scheme with the minmod limiter to allow up to second order accuracy; 3) implicit scheme with local time stepping; 4) Sutherland law for the viscosity and kinetic theory for viscosity and diffusion for one- and multispecies flows, respectively; 5) two-temperature model for nitrogen flow; and 6) no-slip isothermal wall conditions.

The computational grid was multiblock structured, and the cells were stretched to the wedge surface to enhance spatial resolution of the boundary layer.

## Argon Flow

The first set of computations was performed for an argon flow. From the viewpoint of real gas effects, this is the simplest case, which can serve as a reference point for subsequent study of a more complex nitrogen flow.

Typical patterns of an argon flow about a wedge are presented in Fig. 1, where the Mach number fields obtained by DSMC computations are plotted for different values of the wedge angle $\delta_w$. Parts of the flow where the Mach number is within $0.99 < M < 1.01$ have the white color; this allows one to see the position of the sonic line. For a wedge angle of 36 deg, the oblique shock wave is attached to the wedge, and the flow is supersonic everywhere except inside boundary layer. The shock wave is straight until it is affected by the expansion fan at the trailing edge of the wedge. As the wedge angle is increased to 37 deg, the flow pattern becomes completely different: a subsonic region is formed behind the wave, and the wave itself is noticeably curved. In fact, the wave is already detached, though its front cannot be rigorously distinguished from the boundary layer in the plane of symmetry (lower boundary of the domain). For a wedge angle of 46 deg, a flow with a bow shock wave and a large subsonic region behind the wave is formed. The standoff distance is more than 20% of the wedge length. The accuracy of the DSMC results is discussed in the next section; special emphasis is laid on the accuracy of standoff distance determination.

#### Accuracy of DSMC Results

The following conditions should be satisfied for accurate DSMC simulation of the gas flow:

1) The time step should be smaller than the local mean time between collisions and residence time (ratio of the linear size of the collisional cell to the mean molecular speed).

2) The linear size of the collisional cell should be smaller than the local mean free path.

3) The elementary volume whose side is equal to the local mean free path should contain more than one modeling particle [19].

These conditions guarantee that the error associated with time and space discretization and the error related to the finite number of particles in the system are small.

According to these requirements, more than 70 million modeling particles should be used for accurate DSMC modeling of an argon flow around a wedge (for a wedge angle $\delta_w = 46$ deg). Even with the use of supercomputers, manipulation with this number of particles is rather difficult from the computational point of view. Therefore, the sensitivity of DSMC modeling results to the number of modeling particles was considered.

Figure 2 shows the density distributions along the stagnation streamline for a wedge angle $\delta_w = 46$ deg in the series of computations with increasing number of modeling particles and collisional cells. The flow direction coincides with the direction of the $X$-axis, and $x = 0$ corresponds to the stagnation point. The number of particles was approximately $1.1 \times 10^6$ in the first computation of this series and was increased fourfold in each next computation. The number of collisional cells in all computations was approximately four times smaller than the number of particles. In the last computation of the series, $72 \times 10^6$ particles were used. Obtaining of this result required more than two days of computer time with the use of 200 processors. As the number of modeling particles increases from $1.1 \times 10^6$ to $18 \times 10^6$ (see Fig. 2), the shock wave standoff distance increases, and the boundary-layer thickness decreases. With further increase in the number of particles up to $72 \times 10^6$, however, the density profile remains unchanged.

Figure 3 shows the density for the same series of computations in a cross section perpendicular to the wedge plane and passing through the trailing edge of the wedge. The distance from the shock wave front to the wedge plane in this cross section increases with increasing number of particles, as in the case along the stagnation streamline. There is practically no difference between the density distributions for $18 \times 10^6$ and $72 \times 10^6$ particles.

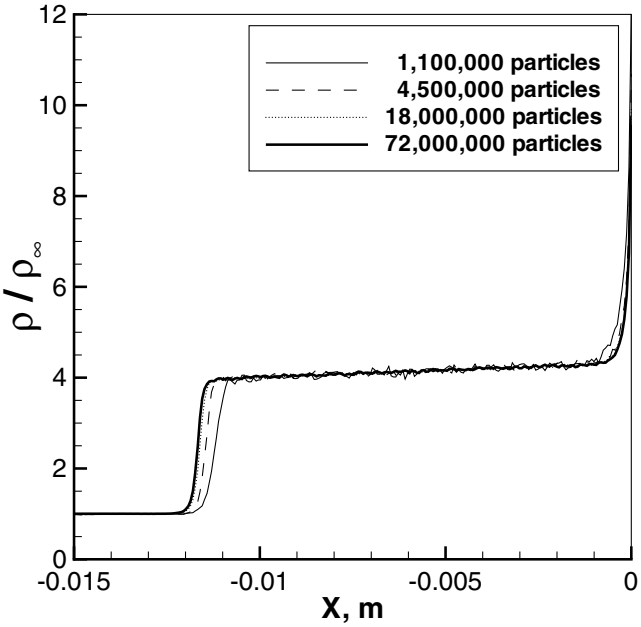


**Fig. 2 Density along the stagnation streamline computed with DSMC. Argon flow, $\delta_w = 46$ deg.**

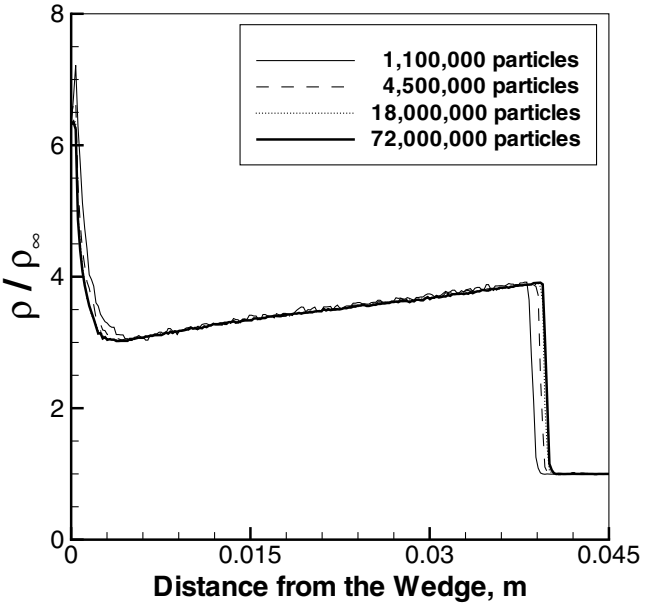


**Fig. 3 Density along the wedge surface normal at the trailing edge computed with DSMC. Argon flow, $\delta_w = 46$ deg.**

Thus, all the DSMC results for the argon flow described next were obtained with the use of approximately $20 \times 10^6$ particles in the system, which is sufficient for obtaining accurate results (in particular, precise determination of the standoff distance).

### Accuracy of NS Results

NS computations with different numbers of cells show that the main result of the increase in the number of cells is the change in the bow-shock thickness. The boundary-layer thickness also becomes different, which is clearly seen in the distribution of parameters along the stagnation streamline for $50 \times 100$, $100 \times 200$, and $200 \times 400$ grids shown in Fig. 4. Further increase in the number of cells ($400 \times 800$) has no effect on the boundary-layer parameters and bow-shock position. The bow-shock thickness becomes different in magnitude but remains unchanged in terms of the number of cells

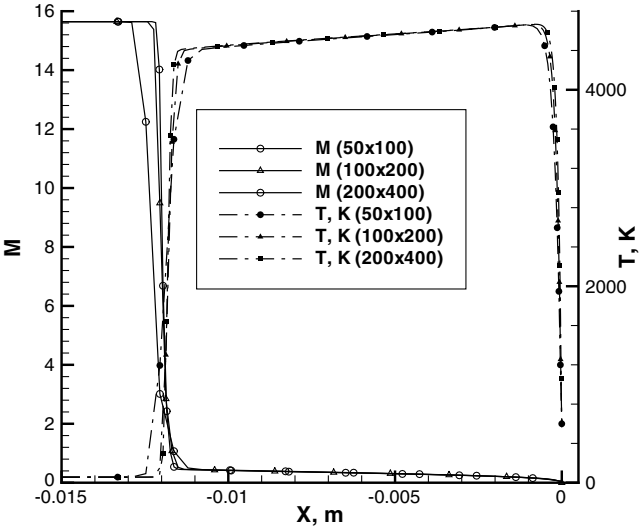


**Fig. 4 Flow parameters along the stagnation streamline computed with NS. Argon flow, $\delta_w = 46$ deg.**

(~5 cells). Therefore, the NS results described next were obtained for the $200 \times 400$ grid.

### Comparison of the NS and DSMC Results

Mach number fields obtained by DSMC (flood) and NS (curves) computations for a wedge angle of 46 deg are compared in Fig. 5. The kinetic and continuum approaches predict similar flow pattern, in particular, the bow-shock position is identical in both cases. An insignificant difference in Mach numbers is observed far from the plane of symmetry. Flowfields of other macroparameters (density, temperature, pressure, velocity, etc.) for both methods also coincide. For a more detailed comparison of DSMC and NS results, the distributions of macroparameters in different cross sections for a wedge angle of 46 deg are presented next.

Figure 6 shows the density and temperature profiles along the stagnation streamline. The NS and DSMC density profiles are in

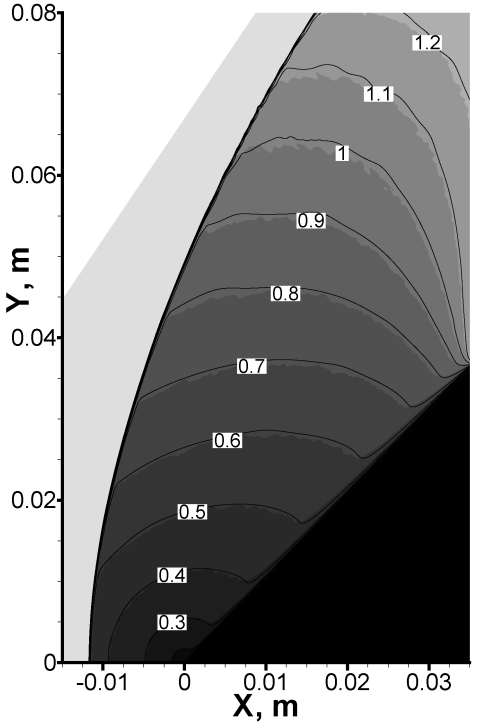


**Fig. 5 Mach number flowfields, DSMC-flood, NS-lines. Argon flow, $\delta_w = 46$ deg.**

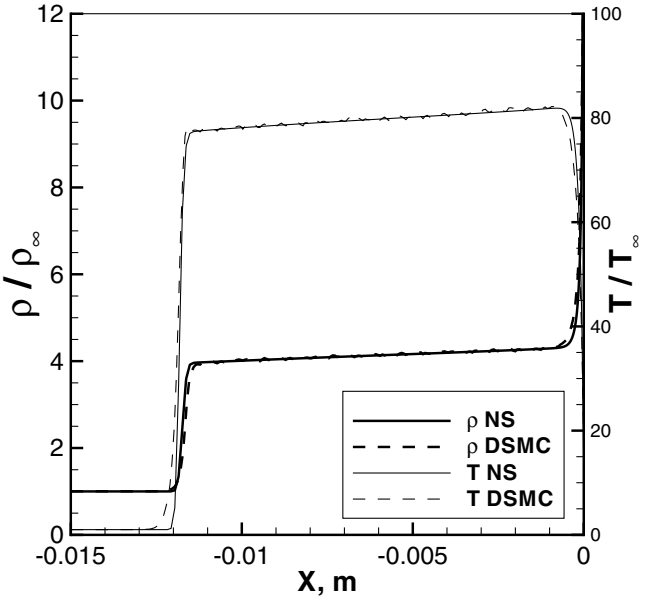


**Fig. 6 Flow parameters along the stagnation streamline. Argon flow, $\delta_w = 46$ deg.**

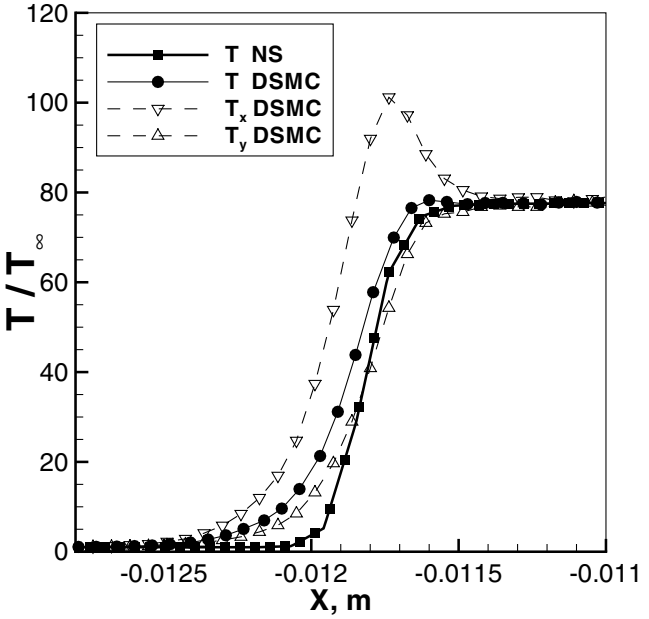


**Fig. 8 Flow parameters along the stagnation streamline. Argon flow, $\delta_w = 46$ deg.**

good agreement. A minor difference in density is observed only in the vicinity of the shock wave front ($x \sim -0.011$ m) and near the stagnation point (inside the boundary layer). The same refers to temperature distributions, except for the fact that the difference between the NS and DSMC temperature profiles in the vicinity of the shock wave front is more pronounced: the NS profile is steeper than the DSMC profile.

Figures 7 and 8 show the NS and DSMC macroparameters along the stagnation streamline in the near vicinity of the shock wave front. The density and velocity profiles are plotted in Fig. 7. One can clearly see that the DSMC density and velocity profiles inside the shock wave front are less steep than the NS profiles. This result could be expected and explained by the commonly known fact that the Navier–Stokes equations cannot correctly describe the internal structure of front of strong shock waves for Mach numbers $M > 2$. The DSMC method offers a detailed description of the internal structure of the front at the kinetic level with account for strong nonequilibrium of the velocity distribution function of molecules.

The nonequilibrium of the distribution function is characterized, in particular, by the strong difference in the values of parallel $T_x$ and perpendicular $T_y$ temperatures whose profiles are plotted in Fig. 8 together with DSMC and NS temperature curves. The parallel temperature has a clearly expressed maximum inside the front. As a whole, the temperature profile obtained by DSMC simulations is less steep than the NS temperature profile and has a small maximum, about 1% of the temperature value behind the wave. The presence of this maximum in strong shock waves in monatomic gases is a well-known fact (see, e.g., [12]).

Figure 9 shows the density and temperature profiles in a cross section perpendicular to the wedge plane and passing through the trailing edge of the wedge. The DSMC and NS values are in very good agreement, except for a small difference in the vicinity of the trailing edge. Both methods also predict an identical distance from the wedge to the shock wave front in this cross section.

As a whole, we can conclude that the results of DSMC simulations are in excellent agreement with the solution of the Navier–Stokes

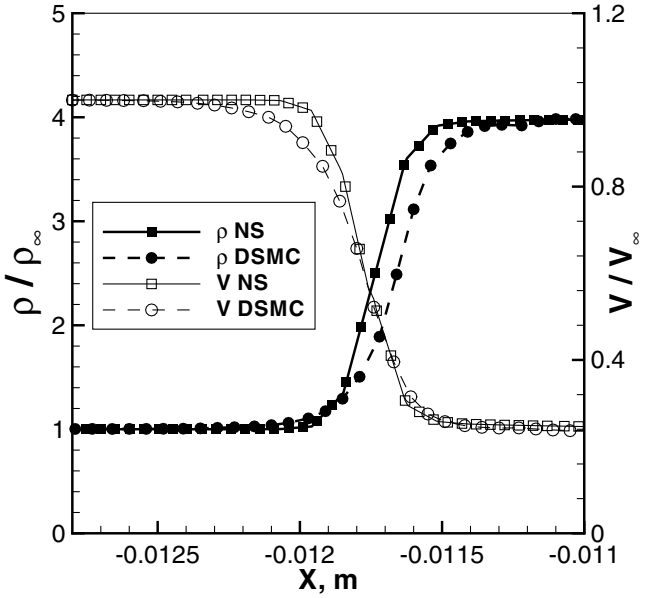


**Fig. 7 Flow parameters along the stagnation streamline. Argon flow, $\delta_w = 46$ deg.**

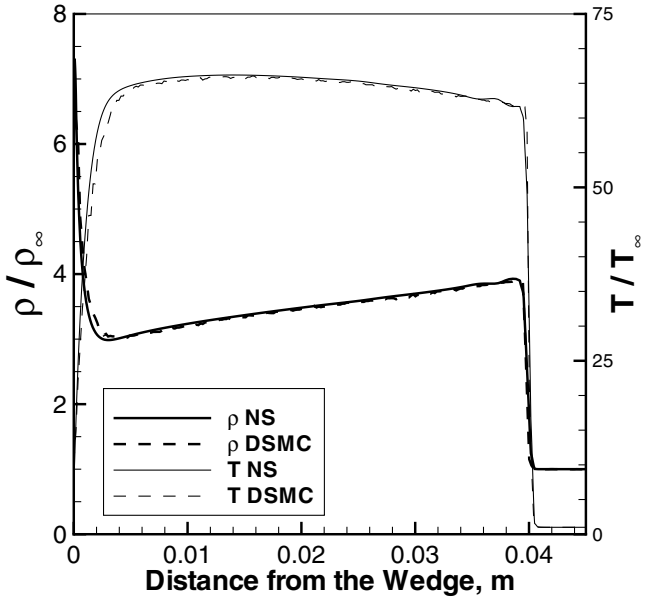


**Fig. 9 Flow parameters along the wedge surface normal at the trailing edge. Argon flow, $\delta_w = 46$ deg.**

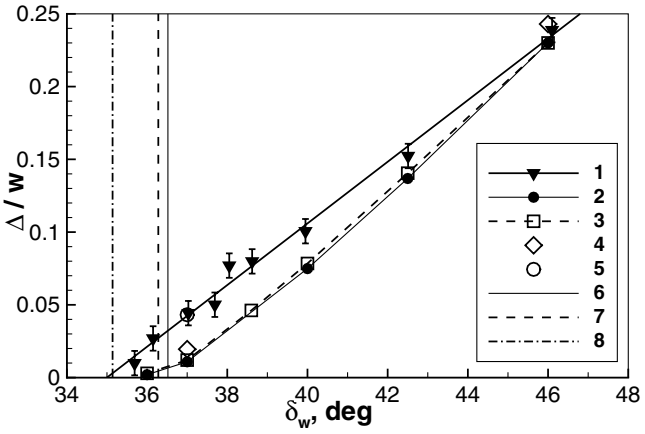


**Fig. 10 Standoff distance. 1–[14]; 2–DSMC; 3–NS; 4–NS for $M = 12$; 5–DSMC for $M = 7$; 6, 7, and 8–detachment angles $M = 15.64$, $M = 12$, and $M = 7$, respectively.**

equations outside the shock wave front and boundary layer. Note, the differences observed inside the shock wave front are not important in the problem considered, and, because of the small thickness of the shock wave front, have not any significant effect on the accuracy of standoff distance determination.

#### Comparison of Numerical Results and Experimental Data

As was mentioned, Hornung and Smith [14] measured the standoff distance of the shock wave for a hypersonic argon flow with different wedge angles. The results of these measurements and the values of the standoff distance obtained by NS and DSMC computations are plotted in Fig. 10. Note the good agreement between the NS and DSMC values of the standoff distance in the entire range of wedge angles for which the computations were performed. Some minor differences are observed for wedge angles of 40 and 42.5 deg only.

A comparison with experimental data shows that the computations significantly underpredict the standoff distance, especially for small wedge angles (more than 3% of the wedge length). For all wedge angles except for 46 deg, the computation results are outside the measurement error of the standoff distance in the experiment (see [14]). Apparently, the reason for this difference is caused by the lack of knowledge of the exact Mach number value at the nozzle exit: "... the displacement thickness of the nozzle wall boundary is quite large at this condition, so that the exit Mach number may be significantly reduced" [14].

To evaluate the Mach number effect on the standoff distance, additional NS computations for $M = 12$ (for $\delta_w = 46$ deg and $\delta_w = 37$ deg) and DSMC computations for $M = 7$ ($\delta_w = 37$ deg) were performed. The freestream parameters (velocity, temperature, and density) for these computations with a reduced Mach number were recalculated from the conditions of conservation of mass flow rate and total enthalpy.

It is clearly seen (see Fig. 10) that a decrease in the Mach number increases the standoff distance. In particular, the NS results for $M = 12$ are in somewhat better agreement with experimental data than the results of the basic series of computations. The DSMC computation for $M = 7$ and $\delta_w = 37$ deg predicts the standoff distance completely coincident with the experimental value for this angle.

The dashed vertical lines in Fig. 10 show the theoretical values of the detachment angle (i.e., the maximum angle of flow deflection) for different Mach numbers. One can clearly see that the results of the basic series of NS and DSMC computations are in excellent agreement with the theoretical value of the detachment angle for $M = 15.64$. On the other hand, wave detachment in the experiment occurs at lower wedge angles than those expected for the Mach number $M = 15.64$.

Thus, further research is necessary to clarify the reasons for the difference between the experimental and numerical data. It is also desirable to obtain more detailed information about the experimental facility used in [14].

## Nitrogen Flow

The next stage was to study the influence of relaxation of the internal energy of the gas and chemical reactions on the flow structure around the wedge. The dissociating nitrogen flow pattern for different wedge angles is demonstrated by the Mach number flowfields plotted in Fig. 11. For an angle of attack of 47 deg, the flow pattern with an attached wave is formed. For a wedge angle of 53.5 deg, one can observe the flow pattern with a slightly detached shock wave. The standoff distance of the wave for a wedge angle of 62.5 deg is about 15% of the wedge length. The main qualitative difference of the flowfields of dissociating nitrogen from those of argon is the shape of isolines immediately behind the shock wave front (cf. Figs. 1 and 11). The Mach number behind the shock wave front in the monatomic gas decreases monotonically with increasing distance from the front. In dissociating nitrogen, the Mach number behind the shock wave first slightly increases and then gradually decreases. The growth of the Mach number behind the shock wave front is associated with relaxation processes (relaxation of internal energy and dissociative relaxation) behind the front (see [14]).

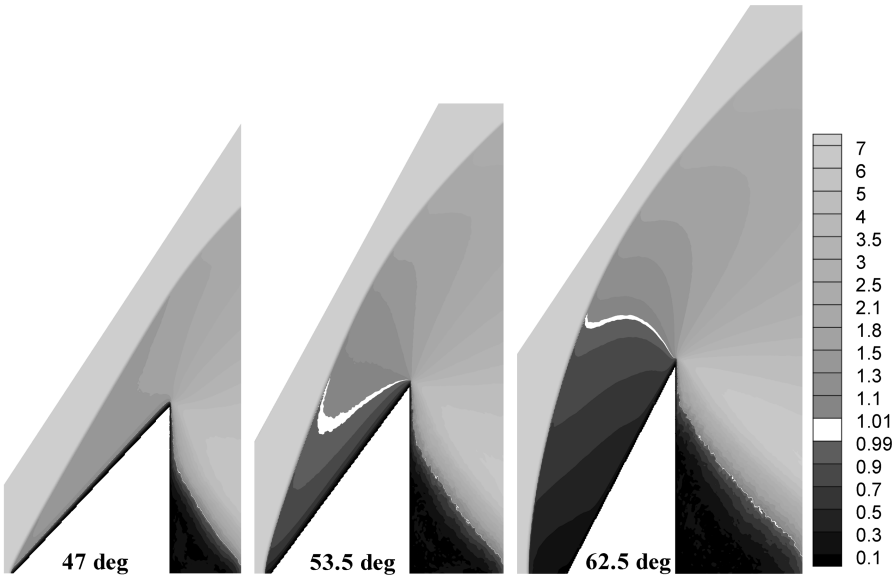


**Fig. 11 Mach number flowfields for different wedge angles (reacting nitrogen flow).**

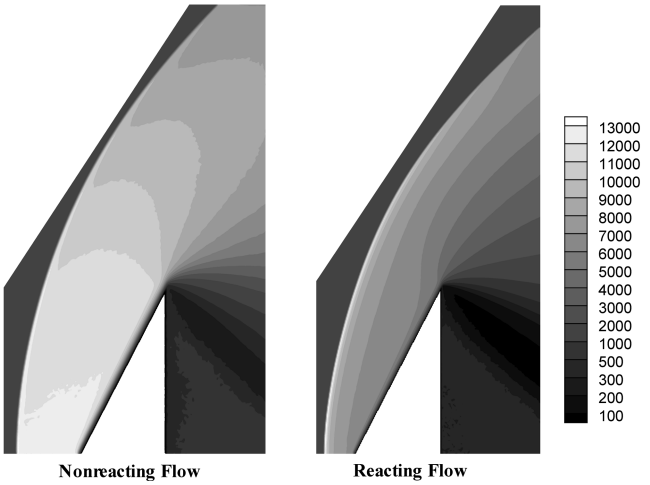


**Fig. 12 Translational temperature flowfields for the nitrogen flow, $\delta_w = 62.5$ deg.**

Two cases were considered to obtain an independent effect of relaxation of internal energy of molecules and dissociation on the flow: 1) nonreacting flow with excitation of internal degrees of freedom of molecules, and 2) reacting flow with excitation of internal degrees of freedom of molecules. Figure 12 shows the fields of translational temperature for the flow with a strongly detached shock wave ($\delta_w = 62.5$ deg) for these two cases. Chemical reactions significantly decrease the temperature behind the shock wave front. The most important fact for this study is that the chemical reactions lead to an approximately twofold decrease in the standoff distance. In the next two subsections, DSMC results with continuous and discrete internal energy models and NS results are compared separately for these two cases.

### Nonreacting Flow

A comparison of density and translational temperature along the stagnation streamline for a wedge angle of 62.5 deg is shown in Fig. 13. All three density profiles (DSMC profiles for both models and NS profile) coincide fairly well except for two regions. The first one is the vicinity of the stagnation point, where the NS computation predicts a slightly smaller boundary-layer thickness than the DSMC method. The second region is the vicinity of the shock wave front where the difference primarily refers to the position of the front itself. The NS computation predicts the greatest standoff distance. The standoff distance for DSMC results with the continuous model is slightly smaller than in NS results. The smallest standoff distance is predicted by the DSMC computation with the discrete model. Note, all differences in the standoff distance between three profiles are within 5%.

All three profiles of translational temperature are also in good agreement almost along the entire stagnation streamline. As in the case of density, there are little differences in the vicinity of the stagnation point. The value of translational temperature behind the shock wave front in the DSMC computation with the discrete model is slightly lower on the average than that in NS and DSMC with the continuous model. The DSMC temperature distributions with the continuous and discrete models also differ in the wave front position (different standoff distance). The differences between the DSMC results for the nonreacting flow with the use of different models can be explained comparing the distributions of the specific heat ratio $\gamma$ along the stagnation streamline. There are several different ways to define the parameter $\gamma$ for a real gas, which are equivalent for the case of a calorically perfect gas (see [20]). One of these definitions is used in the present paper, where the specific heat ratio is understood as the ratio of enthalpy and internal energy of the gas

$$\gamma = \frac{h}{e} = 1 + \frac{2}{\xi}$$

This definition is the most convenient one for the DSMC method, because it allows one to calculate $\gamma$ for a nonreacting gas with excited internal degrees of freedom directly via the average number of effective degrees of freedom. Note that the definition of the specific heat ratio as $1 + 2/\xi$ can also be used in the DSMC method for reacting flows; in the latter case, however, it is not equal to the ratio of enthalpy and internal energy.

The contours of the specific heat ratio along the stagnation streamline are shown in Fig. 14. The specific heat ratios behind the shock wave front are somewhat different for DSMC computations with the continuous and discrete models. This is because in contrast to the continuous model derived for a simple harmonic oscillator (SHO), the discrete model takes into account anharmonicity of molecular vibrations (anharmonicity parameter of 0.82 was used for $N_2$ molecules), and the number of effective vibrational degrees of freedom (and hence, the specific heat ratio) is different in these two models for an identical temperature. Note that the SHO model is also used in the NS computations, which is the reason for the agreement of NS and DSMC-continuous results.

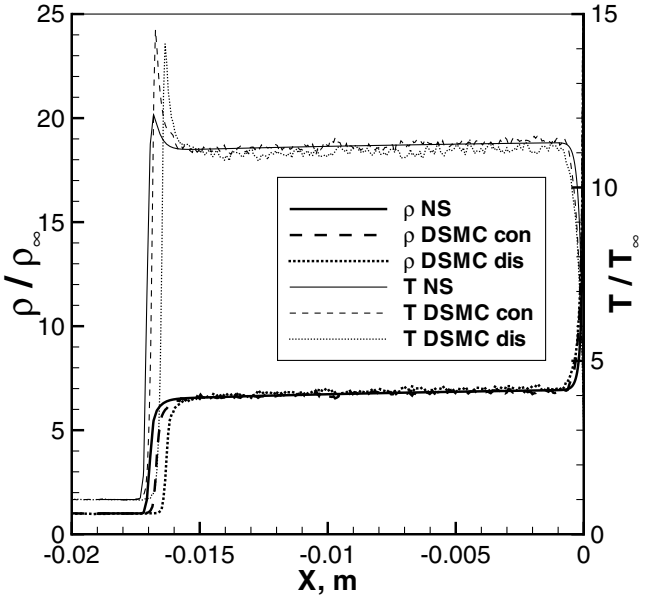


**Fig. 13 Flow parameters along the stagnation streamline. Nonreacting nitrogen flow, $\delta_w = 62.5$ deg.**

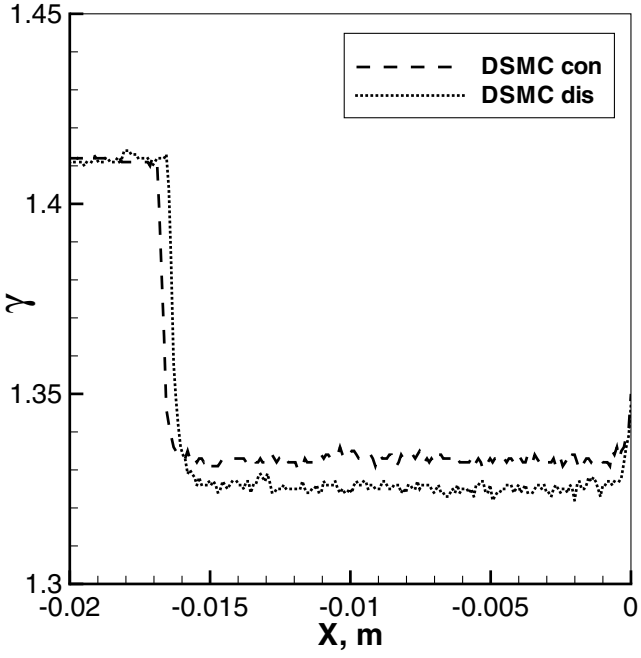


**Fig. 14 Flow parameters along the stagnation streamline. Nonreacting nitrogen flow, $\delta_w = 62.5$ deg.**

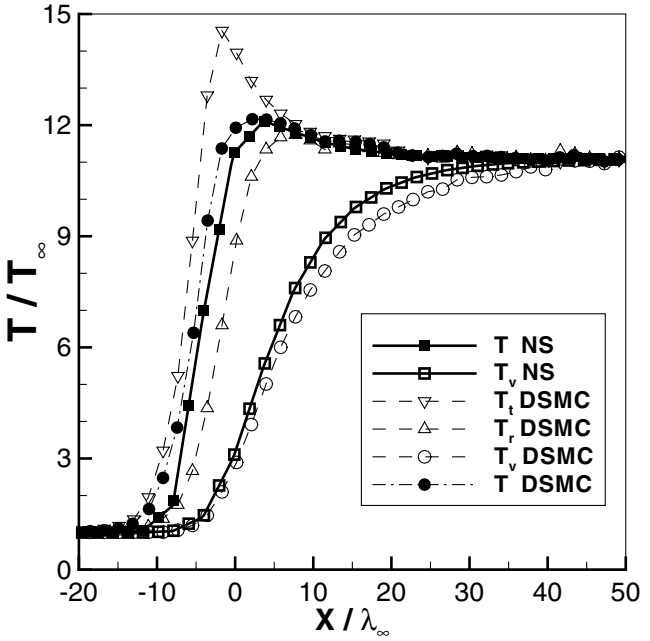


**Fig. 15 Temperatures along the stagnation streamline for the nonreacting flow, $\delta_w = 62.5$ deg.**

The largest difference in the translational temperature distribution (see again Fig. 13) between the NS and DSMC results is observed in the vicinity of the shock wave front. The main difference of the NS temperature distributions from that of the DSMC results with the continuous model is a significantly lower value of the temperature maximum inside the shock wave front.

Let us consider the shock wave front structure in more detail. Figure 15 shows the distributions of various temperatures for NS computations and DSMC computations with the continuous model in the coordinate system fitted to the center of the shock wave front. By definition, the center of the shock wave front is the point where the density equals the halved sum of densities upstream of the front and immediately behind the front. The $x$-coordinate in Fig. 15 is normalized to the freestream mean free path. The reason for the difference in the maximum value of translational temperature for NS and DSMC computations (denoted in the figure as $T$ for NS and $T_t$ for DSMC results, respectively) occurs owing to the fact that, in contrast to the DSMC internal energy models, the two-temperature model used in NS computations ignores the difference in temperature of translational and rotational modes. Hence, the value of translational temperature in NS computations should be treated as the mean value of temperature of translational and rotational molecular modes (the mean value is taken with weights equal to the number of degrees of freedom of the corresponding mode). It is clearly seen that the DSMC values of rotational temperature ($T_r$ DSMC) inside the shock wave front are significantly lower than those of translational temperature. Therefore, the mean temperature of translational and rotational modes ($T$ DSMC) is significantly lower than translational temperature and is in good agreement with $T$ NS in terms of the maximum value.

It should also be noted that the DSMC and NS curves for vibrational temperature ($T_v$ DSMC and $T_v$ NS, respectively) are fairly close (the DSMC profile is slightly less steep). Thus, we can conclude that NS computations and DSMC computations with the continuous model predict a similar vibrational relaxation length. This is explained by the use of similar models for vibrational energy and vibrational relaxation in DSMC (continuous model) and NS computations: SHO model for molecular vibrations, temperature-dependent vibrational collision numbers (Millikan–White expression [21]), and Landau–Teller relaxation equation (this equation is not used explicitly in DSMC computations, but the DSMC models of translational-vibrational energy transfer is constructed in such a way that the relaxation rates satisfy the Landau–Teller equation in equilibrium).

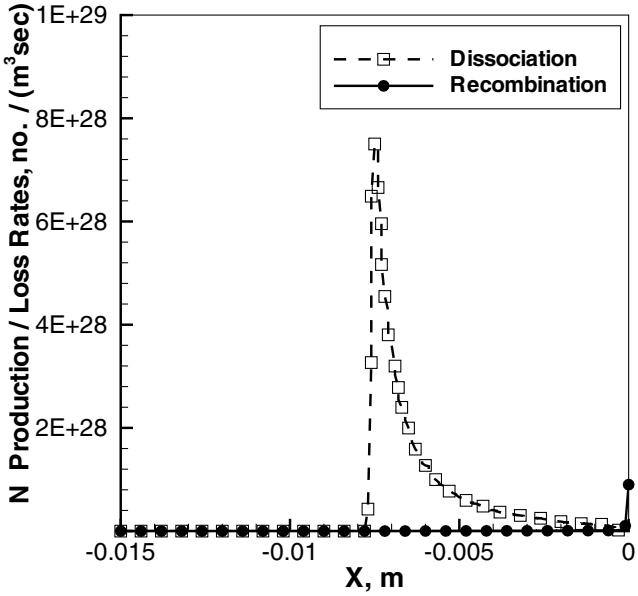


**Fig. 16 Atomic nitrogen production/loss rate due to dissociation/recombination along the stagnation streamline, $\delta_w = 62.5$ deg.**

**Reacting Flow**

Recall that only dissociation reactions were taken into account in the present work. Indeed, under conditions considered, dissociation makes the main contribution to the flow properties. Figure 16 shows the estimate of the rates of production and loss of atomic nitrogen due to dissociation and recombination, respectively, along the stagnation streamline. This estimate is based on flow parameters obtained by DSMC simulation of the dissociating nitrogen flow. The chemical reactions in the estimate were assumed to follow the Arrhenius law [Eq. (1)] where the overall kinetic temperature of the flow (see [12]) is used as $T$. This estimate shows that recombination occurs only inside the boundary layer.

Figure 17 shows the distributions of density and translational temperature for a chemically reacting flow for a wedge angle of 62.5 deg, obtained by NS and DSMC computations with both models. As for a nonreacting flow, the use of the discrete model yields a smaller shock wave standoff distance. DSMC results with different models of real gas effects differ significantly in the vicinity of the shock wave front and in a certain region immediately behind the front. Both the density and translational temperature distributions

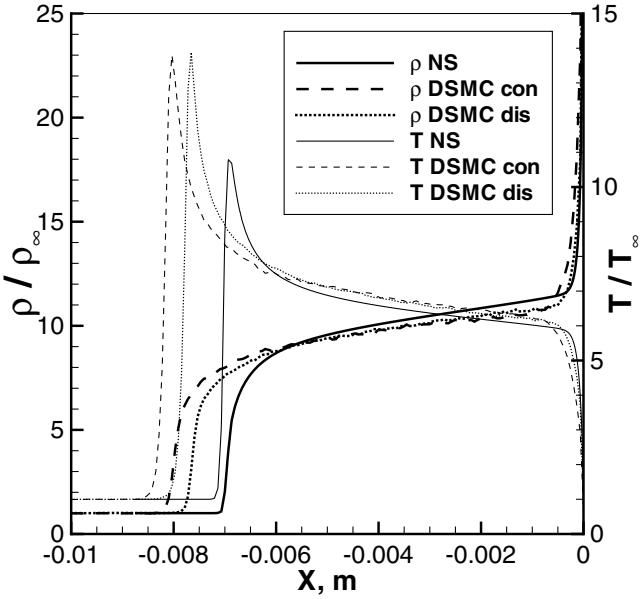


**Fig. 17 Flow parameters along the stagnation streamline. Reacting nitrogen flow, $\delta_w = 62.5$ deg.**

show that the differences in NS and DSMC results are more substantial, as compared to the nonreacting flow. In addition to the difference in the maximum value of translational temperature (which can be explained by the same reason as for the nonreacting flow) and differences inside the boundary layer, there are also differences along the entire stagnation streamline, namely, NS computations yield a faster decrease in temperature and increase in density behind the shock wave front and also a significantly smaller standoff distance (by more than 10%) than in DSMC computations.

A comparison of the distributions of the atomic nitrogen mass fraction for the same computations is shown in Fig. 18. DSMC computations with different models of real gas effects yield a qualitatively identical result, and the main differences are related to the different value of the standoff distance (mass fraction of N starts to grow earlier in DSMC computations with the continuous model). NS computations predict a significantly sharper increase in the mass fraction of N inside the shock wave front than DSMC computations. Immediately behind the front, vice versa, the increase in the mass fraction of N is less steep in NS computations than in DSMC computations. Thus, we can conclude that the difference between the chemical reaction models used in DSMC and NS computations is substantial.

There is also a qualitative difference near the stagnation point: NS computations predict a constant value of the mass fraction of N, whereas the latter decreases near the wall in DSMC computations. Apparently, this difference can be attributed to the different description of diffusion processes in two approaches. A more detailed analysis of the reasons for these differences is planned for the future.

#### Effect of the Vibration-Dissociation Coupling

In this subsection the results of reacting flow computations with the discrete model are compared with the results obtained using the VDC model. The VDC model has a free nonnegative parameter $\phi$, which determines the degree of vibrational favoring: the greater $\phi$, the greater this degree. If $\phi = 0$, the model still has some degree of vibrational favoring and is not equivalent to the discrete model. The values of the VDC parameter $\phi = 0$, 1, and 3 were used in the present study (in what follows, cases with these values of the VDC parameter are denoted by VDC0, VDC1, and VDC3, respectively).

The profiles of translational temperature for VDC0, VDC1, VDC3 and discrete (reacting and nonreacting) cases for a wedge angle of 62.5 deg are plotted in Fig. 19. The minimum standoff distance is observed in computations for reacting case with the discrete model (about 8 mm). In computations with the VDC model, the standoff distance is greater; as the VDC parameter $\phi$ increases from 0 to 3, the standoff distance increases approximately from 9 to 11.5 mm. The standoff distance reaches the highest value (approximately 17 mm) in the nonreacting case. In all four reacting cases (discrete and VDC), the temperature decreases behind the shock wave front. The most intense decrease in temperature is observed in the discrete reacting case. For the VDC model, the temperature behind the wave decreases less drastically than that in the discrete reacting case; the higher the value of the VDC parameter, the less significant decrease in temperature behind the wave. In the nonreacting case, the temperature behind the shock wave front reaches a constant value and decreases only in the vicinity of the stagnation point (inside the boundary layer). These results can be explained by the fact that the higher the degree of vibration-dissociation coupling in the model of chemical reactions, the slower the dissociation behind the shock wave front, and hence, the closer the results to the nonreacting case.

This conclusion is supported by the profiles of atomic nitrogen mass fractions for all four reacting cases also shown in Fig. 20. Indeed, the atomic nitrogen mass fraction behind the shock wave reaches the maximum value equal to 0.33 in the discrete reacting case. With the use of the VDC model, the maximum values of the mass fraction do not exceed 0.31, 0.30, and 0.27 for $\phi = 0$, 1, and 3, respectively. Thus, allowance for vibration-dissociation coupling reduces the rate of dissociation behind the shock wave front.

#### Comparison of Numerical Results and Experimental Data

The experimental and numerical curves for the standoff distance vs the wedge angle for a nitrogen flow are plotted in Fig. 21. First, note that the computations predict an almost linear dependence of the standoff distance on the wedge angle for the nonreacting gas. DSMC simulation results for the nonreacting gas with the use of the continuous model are in very good agreement with NS results for several values of the wedge angle. The standoff distance is somewhat smaller when the discrete model is used in the DSMC simulations.

Chemical reactions in the numerical modeling, both NS and DSMC, result in a slower and nonlinear increase in the standoff distance with increasing wedge angle. NS results predict an interval of the nonlinear increase in the standoff distance from 47 to 56.5 deg. For wedge angles greater than 56.5 deg, the standoff distance increases almost linearly in NS computations. DSMC computations

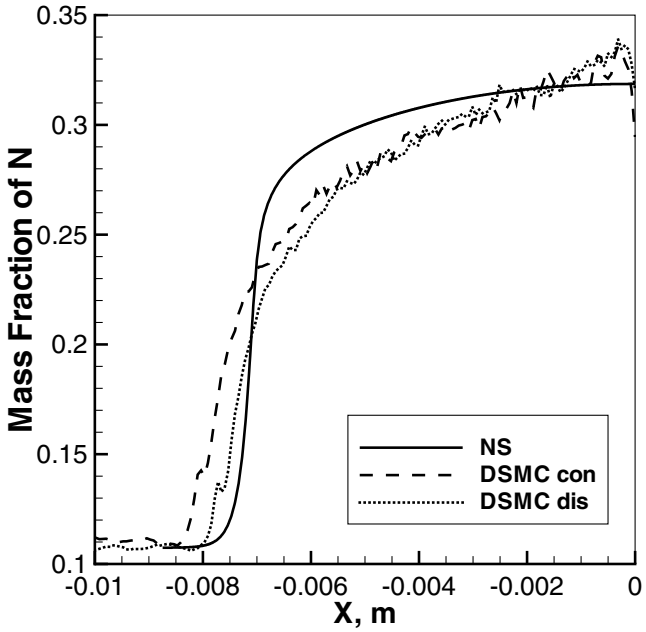


**Fig. 18 Flow parameters along the stagnation streamline. Reacting nitrogen flow, $\delta_w = 62.5$ deg.**

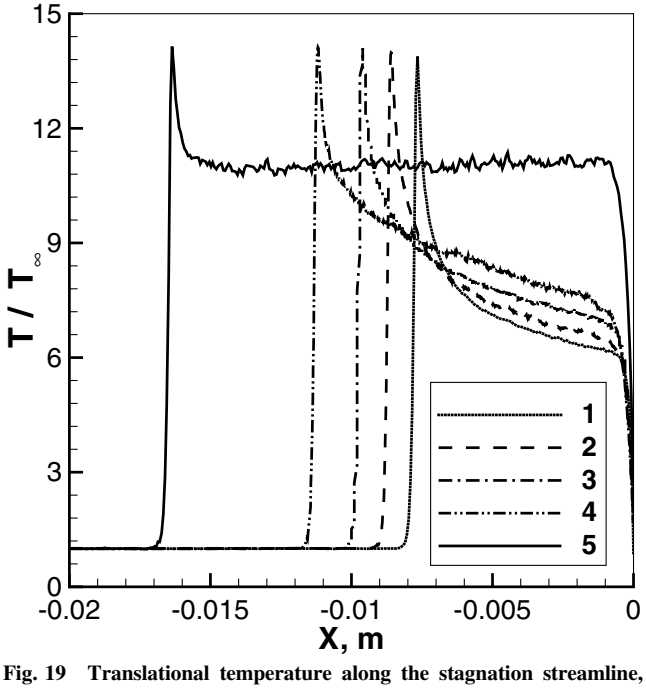


**Fig. 19 Translational temperature along the stagnation streamline, $\delta_w = 62.5$ deg. 1–discrete, 2–VDC0, 3–VDC1, 4–VDC3, 5–discrete (nonreacting).**

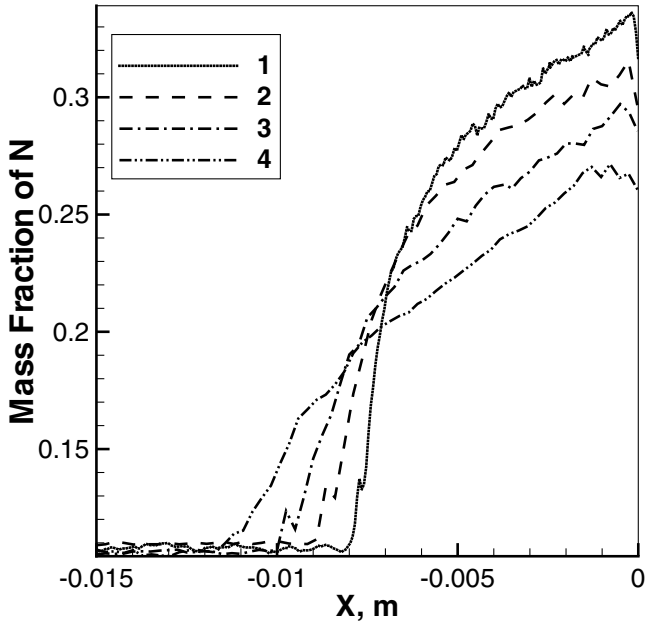


**Fig. 20 Atomic nitrogen mass fraction along the stagnation streamline, $\delta_w = 62.5$ deg. 1–discrete, 2–VDC0, 3–VDC1, 4–VDC3.**

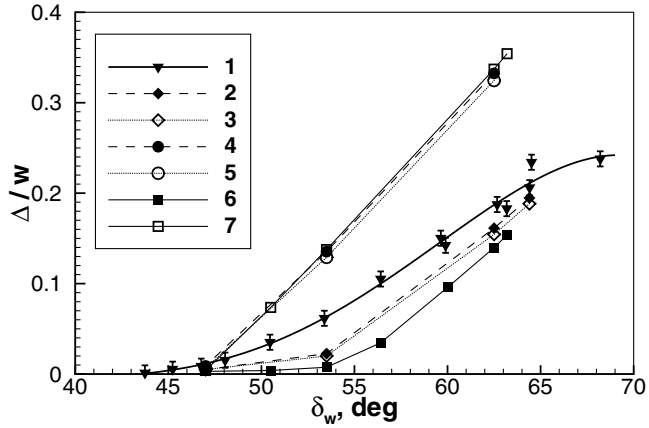


**Fig. 21 Standoff distance. 1–[14], 2–DSMC for reacting flow (continuous), 3–DSMC for reacting flow (discrete), 4–DSMC for nonreacting flow (continuous), 5–DSMC for nonreacting flow (discrete), 6–NS for reacting flow, 7–NS for nonreacting flow.**

for the reacting flow predict a dependence of the standoff distance on $\delta_w$, which coincides qualitatively with NS results, though the DSMC method yields a noticeably greater standoff distance than NS computations in the entire range of wedge angles. As in the nonreacting case, the standoff distance is slightly smaller if the discrete model of real gas effects is used in DSMC computations than for the continuous model.

A comparison of numerical simulation results for the reacting gas with the standoff distance measured in the experiment of [14] shows that numerical simulations offer a qualitatively correct description of the nonlinear dependence of the standoff distance on the wedge angle, which is in agreement with the conclusions of [14]. Note, nevertheless, a significant quantitative difference between the computational results and experimental data. First, the computations, both DSMC and NS, predict detachment at a higher wedge angle ($\delta_w > 47$ deg) than the experiment ($\delta_w \sim 45$ deg). Second, the computations underpredict the standoff distance. Almost for all values of the wedge angle, the computation results are outside the measurement error for the standoff distance.

When the VDC model is used, the standoff distance increases, as compared to the discrete case (see Fig. 22). The higher the VDC

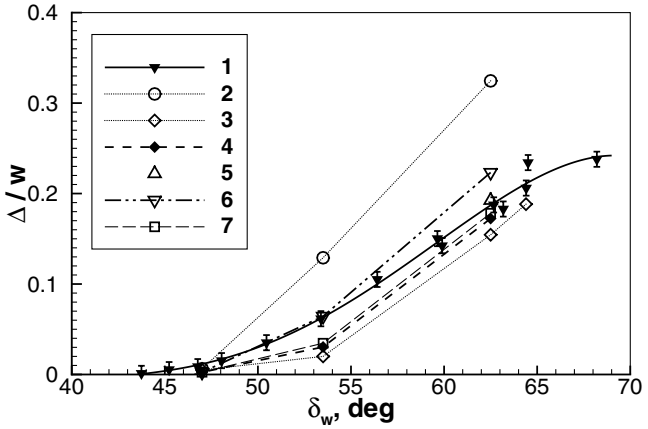


**Fig. 22 Standoff distance. 1–[14], 2–DSMC for nonreacting flow (discrete), 3–DSMC for reacting flow (discrete), 4–DSMC for reacting flow (VDC0), 5–DSMC for reacting flow (VDC1), 6–DSMC for reacting flow (VDC3), 7–DSMC for reacting flow (discrete, reaction rates of [16]).**

parameter, the greater the standoff distance, which is illustrated by computations for wedge angles of 53.5 and 62.5 deg. VDC0 computations yield a result lying slightly outside the measurement-error bar for an angle of 62.5 deg but underpredict the standoff distance for an angle of 53.5 deg almost by a factor of 2. The results of VDC1 computations for an angle of 62.5 deg are within the measurement error. VDC3 computations yield excellent agreement with experimental data for an angle of 53.5 deg but significantly (by more than 15%) overpredict them for a wedge angle of 62.5 deg. Note that the computation results for all cases for an angle of 47 deg predict a flow pattern with an attached shock. This means that the detachment angle for all cases considered is not smaller than 47 deg, which is approximately 2 deg higher than in the experiment. Another significant difference of the computation results for all reacting cases from experimental data is a more rapid growth of the standoff distance with increasing wedge angle (for $\delta_w > 53.5$ deg).

Figure 22 also shows the results of modeling with the discrete model and reaction rates of [16]. One can clearly see that the use of alternative reaction rates leads to a certain increase in the standoff distance for angles of 53.5 and 62.5 deg but does not eliminate the difference between numerical results and experimental data, which were mentioned in preceding paragraphs.

Because the computation results for the dissociating nitrogen flow, as for the argon flow, underpredict experimental data, some uncertainty in freestream conditions is also possible for the nitrogen flow. A more profound study of the chemically reacting nitrogen flow around the wedge and a more detailed analysis of the reasons for the difference in computational and experimental results are necessary.

## Conclusions

A steady hypersonic 2-D flow around a wedge with a Knudsen number $Kn \sim 5 \times 10^{-4}$ was numerically studied by the kinetic, DSMC method, and continuum, Navier–Stokes equations, approaches both for a monatomic gas, argon, and a diatomic reacting and nonreacting gas, nitrogen. Three models of real gas effects were used in DSMC computations of the nitrogen flow: continuous model, discrete model, and a model which takes into account the effect of vibration-dissociation coupling. The DSMC computations were performed on a multiprocessor computer MVS1000M using up to 200 processors and up to 70 million modeling particles.

Very good agreement was obtained between DSMC results for the argon flow and the numerical solution of the Navier–Stokes equations in a wide range of wedge angles. The differences are observed inside the shock wave front only. Numerical results underpredict the experimentally measured standoff distance of the shock wave. The most probable reason for this distinction can be the

difference between actual freestream conditions in the experiment and the values cited in [14]

A comparison of the numerical solution of the Navier–Stokes equations (with the two-temperature model) for the nonreacting nitrogen flow with the results of DSMC simulations (with the use of discrete and continuous models of real gas effects) reveals their good agreement. DSMC computations for reacting nitrogen predict a greater standoff distance than NS computations. A detailed comparison of results shows that the chemical reactions in NS modeling proceed much faster than in the DSMC approach. Therefore, a detailed analysis of the models of chemical reactions used in the CFD-FASTRAN NS solver is needed.

Numerical results for the nonreacting nitrogen flow predict a linear increase of the standoff distance with increasing wedge angle. Chemical reactions in numerical modeling result in a nonlinear dependence of the standoff distance on the wedge angle, which is in qualitative agreement with experimental data. Quantitatively, the numerical simulation results overpredict the detachment angle and underpredict the standoff distance obtained in experiments.

The simulation results show that vibration-dissociation coupling decreases chemical reaction rates behind the shock wave, which yields a significantly greater standoff distance. The account for the coupling also improves the agreement between numerical and experimental data on the standoff distance for some values of the wedge angle. Nevertheless, for all fixed values of the VDC parameter, the computed dependence of the standoff distance on the wedge angle significantly differs from the experimental one. First, detachment occurs at an angle approximately 2 deg higher than that in the experiment; second, the computations predict a more rapid growth of the standoff distance with wedge angle.

The influence of the reaction rate constant on modeling results was also examined. The standoff distance somewhat increases when alternative reaction rates [16] are used, but the difference from experimental data is still considerable. Similar to the argon flow, additional analysis of the freestream conditions and further numerical studies are necessary to elucidate this discrepancy.

## Acknowledgments

The research conducted at ITAM was performed under RFBR Grant No. 03-07-90403, No. 03-01-00244, and No. 03-07-90248, ISTC Project 2298p, Program No. 17 for Basic Research of the Russian Academy of Sciences (2003), and Integrated Project of the Siberian Branch of the Russian Academy of Sciences No. 2 (2003). This support is gratefully acknowledged. The authors are grateful to Natalya Gimelshein, whose code was used for calculating chemical reaction probabilities employed in DSMC computations with the discrete and VDC models of real gas effects. Computational resources for the DSMC computations were provided by the Interdepartmental Supercomputer Center (Moscow, Russia). G. N. Markelov thanks Paul Pearson (AOES, The Netherlands) for the computer resources for NS computations, Louis Walpot (AOES, The Netherlands) for fruitful discussions of NS results, and Rohit Jain (CFDRC, US) for the explanations of CFD-FASTRAN features.

## References

[1] Haas, B. L., and Boyd, I. D., "Models for Vibrationally Favoured Dissociation Applicable to a Particle Simulation," AIAA Paper 91-0774, 1991.

[2] Koura, K., "Statistical Inelastic Cross-Section Model for the Monte Carlo Simulation of Molecules with Discrete Internal Energy," *Physics of Fluids A*, Vol. 4, No. 8, 1992, pp. 1782–1788.

[3] Boyd, I. D., "Relaxation of Discrete Rotational Energy Distributions Using a Monte Carlo Method," *Physics of Fluids A*, Vol. 5, No. 9, 1993, pp. 2278–2286.

[4] Gimelshein, S. F., Gorbachev, Y. E., Ivanov, M. S., and Kashkovsky, A. V., "Real Gas Effects on the Aerodynamics of 2-D Concave Bodies in the Transitional Regime," *Proceedings of 19th International Symposium on Rarefied Gas Dynamics*, edited by J. Harvey and G. Lord, Vol. 1, Oxford Univ. Press, Oxford, 1995, pp. 556–563.

[5] Boyd, I. D., "A Threshold Line Dissociation Model for the Direct Simulation Monte Carlo Method," *Physics of Fluids A*, Vol. 8, No. 5, 1996, pp. 1293–1300.

[6] Ivanov, M. S., and Gimelshein, S. F., "Computational Hypersonic Rarefied Flows," *Annual Review of Fluid Mechanics*, Vol. 30, Annual Reviews, Inc., Palo Alto, CA, 1998, pp. 469–505.

[7] Wysong, I. J., Dressler, R. A., Chiu, Y. H., and Boyd, I. D., "Evaluation of DSMC Dissociation Models Through Comparison to Measured Cross Sections," AIAA Paper 2000-2359, June 2000.

[8] Borgnakke, C., and Larsen, P. S., "Statistical Collision Model for Monte Carlo Simulation of Polyatomic Gas Mixture," *Journal of Computational Physics*, Vol. 18, No. 4, 1975, pp. 405–420.

[9] Gimelshein, S. F., Gimelshein, N. E., Levin, D. A., Ivanov, M. S., and Markelov, G. N., "Modeling of Rarefied Hypersonic Flows over Spacecraft in Martian Atmosphere Using the DSMC Method," AIAA Paper 2002-2759, 2002.

[10] Lumpkin, F. E., III, Haas, B. L., and Boyd, I. D., "Resolution of Differences Between Collision Number Definitions in Particle and Continuum Simulations," *Physics of Fluids A*, Vol. 3, No. 9, 1991, pp. 2282–2284.

[11] Gimelshein, N. E., Gimelshein, S. F., and Levin, D. A., "Vibrational Relaxation Rates in the Direct Simulation Monte Carlo Method," *Physics of Fluids*, Vol. 14, No. 12, 2002, pp. 4452–4455.

[12] Bird, G. A., *Molecular Gas Dynamics and the Direct Simulation of Gas Flows*, Clarendon, Oxford, 1994.

[13] Bondar, Y., Gimelshein, N., Gimelshein, S., Ivanov, M., and Wysong, I., "On the Accuracy of DSMC Modeling of Rarefied Flows with Real Gas Effects," *Proceedings of 24th International Symposium on Rarefied Gas Dynamics, AIP Conference Proceedings*, Vol. 762, edited by M. Capitelli, Melville, New York, 2005, pp. 607–613.

[14] Hornung, H. G., and Smith, G. H., "The Influence of Relaxation on Shock Detachment," *Journal of Fluid Mechanics*, Vol. 93, Pt. 2, 1979, pp. 225–239.

[15] Moss, J. N., Bird, G. A., and Dogra, V. K., "Nonequilibrium Thermal Radiation for an Aeroassist Flight Experiment Vehicle," AIAA Paper 88-0081, 1988.

[16] Kewley, D. J., and Hornung, H. G., "Free-Piston Shock-Tube Study of Nitrogen Dissociation,"*Chemical Physics Letters*, Vol. 25, No. 4, 1974, pp. 531–539.

[17] Ivanov, M. S., Markelov, G. N., and Gimelshein, S. F., "Statistical Simulation of Reactive Rarefied Flows: Numerical Approach and Applications," AIAA Paper 98-2669, 1998.

[18] CFD-FASTRAN: User manual, Ver. 2003, CFD Research Corporation, Huntsville, AL, 2003.

[19] Ivanov, M. S., and Gimelshein, S. F., "Current Status and Prospects of the DSMC Modeling of Near-Continuum Flows of Non-Reacting and Reacting Gases," *Proceedings of 23d International Symposium on Rarefied Gas Dynamics, AIP Conference Proceedings*, Vol. 663, edited by A. D. Ketsdever and E. P. Muntz, Melville, New York, 2003, pp. 339–348.

[20] Hayes, W. D., and Probstein, R. F., *Hypersonic Flow Theory*, edited by F. N. Frenkiel, Academic Press, New York, 1959.

[21] Millikan, R. C., and White, D. R., "Systematics of Vibrational Relaxation," *Journal of Chemical Physics*, Vol. 39, No. 12, 1963, pp. 3209–3213.